

## Droplet impact in icing conditions – the influence of ambient air humidity

T. BOBINSKI<sup>1</sup>), G. SOBIERAJ<sup>1</sup>), K. GUMOWSKI<sup>1</sup>), J. ROKICKI<sup>1</sup>),  
M. PSARSKI<sup>2</sup>), J. MARCZAK<sup>2</sup>), G. CELICHOWSKI<sup>2</sup>)

<sup>1</sup>) *Institute of Aeronautics and Applied Mechanics  
Warsaw University of Technology  
Nowowiejska 24, 00-665 Warsaw, Poland  
e-mail: tbobinski@meil.pw.edu.pl*

<sup>2</sup>) *Department of Materials Technology and Chemistry  
University of Łódź  
Pomorska 163, 90-236 Łódź, Poland  
e-mail: mpsarski@uni.lodz.pl*

THE SUBJECT OF THE PRESENT PAPER is the applicability of hydrophobic surfaces for passive anti-icing protection. The experiments were focused on freezing droplets and on various droplet impingement and deformation scenarios. Droplet impact was investigated using high-speed camera for surfaces with different physico-chemical properties. To investigate the difference in droplet behavior on the surfaces with different wettability the steel and the aluminum plates were used and compared with specially designed surfaces characterized by a low surface energy. The influence of air humidity on droplet freezing was confirmed. The effective prevention of icing was observed only if humidity was removed from the system during the experiment.

**Key words:** droplet impingement, freezing of droplets, hydrophobic surfaces, anti-icing application.

Copyright © 2014 by IPPT PAN

### 1. Introduction

THE DYNAMICS OF DROPLET COLLISION with dry or wet substrate has been subject of research since the 19th century. The precursor of such investigation was Worthington [1]. The phenomenon is relevant to many applications, such as industrial painting and agriculture (for example spray cooling, coating, painting, ink-jet printing, spraying of herbicides and pesticides). One of the undesirable effects, related to high-speed droplet impact, is erosion occurring at steam turbines blades. Another cases, in which repelling water properties have to be enhanced include wind-shields and textiles. Recently, application of superhydrophobic coatings to prevent icing on aircrafts has been considered.

If we consider droplet impacting dry and flat surface, three main deformation scenarios can be distinguished (LIU [2], REIN *et al.* [3], YARIN [4]): bouncing, spreading and splashing (Fig. 1). Appearance of certain droplet behavior depends on impact velocity  $U$ , droplet diameter  $D_0$ , and physical properties of water: density, viscosity, surface tension and temperature  $\rho_f$ ,  $\mu_f$ ,  $\sigma_f$ ,  $T_f$ , respectively (subscript  $f$  denotes fluid). In addition, it depends on surface properties like roughness, temperature, liquid film on the surface, wettability (contact angle and contact angle hysteresis).

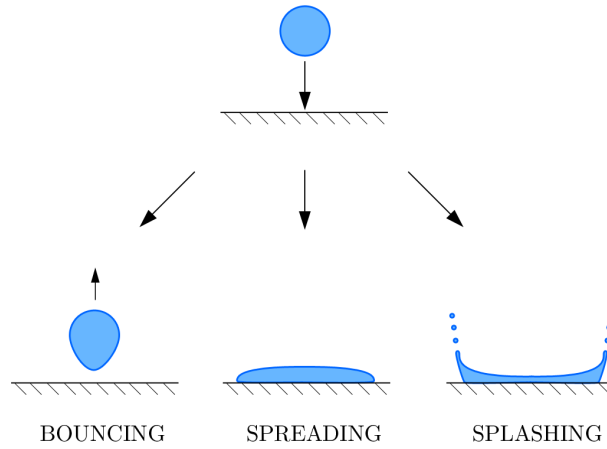


FIG. 1. Droplet deformation scenarios.

The phenomenon of droplet impingement can be described using the following dimensionless parameters:

$$(1.1) \quad \begin{aligned} \text{We} &= \frac{\rho_f U^2 D_0}{\sigma_f}, & \text{Re} &= \frac{\rho_f U D_0}{\mu_f}, & \mathbb{K} &= \text{We} \cdot \text{Oh}^{-2/5}, \\ \text{Oh} &= \frac{\mu_f}{\sqrt{\rho_f \sigma_f D_0}}, & \text{Ca} &= \frac{\mu_f U}{\sigma_f}, & \mathbb{P} &= \text{We}/\text{Re}^{4/5}, \end{aligned}$$

out of which Weber  $\text{We}$  number plays the most important role in the present study (Ohnesorge  $\text{Oh}$  and capillary  $\text{Ca}$  numbers are functions of Reynolds number  $\text{Re}$  and  $\text{We}$ ). CLANET *et al.* [5] defined the impact number  $\mathbb{P}$ , which discriminates between the capillary and viscous regimes (see also BARTOLO *et al.* [6]). The impact number  $\mathbb{P} < 1$  implies negligible influence of viscosity, which permits to treat such a case as inviscid. In case of our experiment this condition was satisfied ( $\mathbb{P} < 0.14$ ).

The freezing process depends on thermal properties of the surface (specific heat  $c_p$ ) and of the fluid (latent heat  $L$ ) as well as on the temperature difference

between the surface and the fluid  $\Delta T$ . These quantities form the dimensionless Stefan number:

$$(1.2) \quad Ste = \frac{c_p \Delta T}{L}.$$

Technical applications of droplet deformation process may require enhanced wettability (e.g., spraying), in other applications it is important to repel water from the surface. Therefore, it is necessary to determine critical conditions for the occurrence of certain droplet deformation scenarios (bouncing, spreading, splashing) as a function of initial parameters [3]. Spreading is associated with surface wettability, while the remaining scenarios may end up with complete recoil existing in bouncing regime or partial rebound, which occurs in bouncing and spreading regimes. Each of the regimes has been extensively investigated in the past. Bouncing was partially analysed by CHEVY *et al.* [7], YUN *et al.* [8], OKUMURA *et al.* [9], VARANASI *et al.* [10] and BARTOLO *et al.* [11]. The reader may find interesting the analysis of spreading regime given by LUNKAD *et al.* [12] and RIOBOO *et al.* [13]. The splashing regime was investigated by ZHANG *et al.* [14] and XU *et al.* [15]. Splashing is attributed by various authors to different causes. Some explain this phenomenon in the context of the Rayleigh–Plateau instability [14], others relate it to the Ritchmyer–Meshkov instability [16], combination of the Rayleigh–Taylor and the Ritchmyer–Meshkov instability [17], a nonlinear amplification mechanism [18] or a gas flow at the edge of the spreading drop [19]. Vast range of splash morphologies was noted; hence, it is possible that each effect can be treated as dominant in a particular parameter regime.

There exist many others papers, not mentioned here, which recently substantially increased the understanding of the phenomenon of droplet collisions, also in the context of icing.

Development of novel materials induced new interest in droplet interaction with textured surfaces coated with different chemical compounds. Static methods of investigating droplets on such surfaces, like determination of droplet static contact angle, roll off angle or contact angle hysteresis, do not provide enough insight into phenomena occurring in industrial applications. To develop icephobic surfaces, it is relevant to have better insight into the frosting mechanism (JUNG *et al.* [20]). Furthermore, applicability of hydrophobic surfaces depends on environmental conditions, which have to be taken into consideration to see their influence on icing.

The anti-icing properties of hydrophobic substrates were confirmed by WANG *et al.* [21]. It was stated that increasing surface hydrophobicity leads to retardation of ice accumulation (heat transferring capability and water-cooling rate decrease). It was also shown by KULINICH *et al.* [22] that, in case of hydrophobic

coating, shear stress needed for ice detachment is several times lower than that on uncoated aluminum or on the flat fluoropolymer surface. In [23] it is shown that value of shear stress needed for ice detachment does not strongly vary with contact angle. However, it was also demonstrated that the critical factor seems to be the hysteresis of the contact angle. To obtain the best anti-icing performance it has to be as low as possible.

The most promising approach consists in application of lubricant-impregnated nanotextured surfaces. On such surfaces droplets become highly mobile and move at speeds that are several orders of magnitude higher than those on identically textured superhydrophobic surfaces. Recently, RYKACZEWSKI *et al.* [24] filled pores of textured surface with perfluorinated oil. It was shown that the process of frost formation is accompanied by migration of the lubricant from within textured surface, which as a result compromises this solution. Currently, no solution to this problem is available.

The main goal of the present paper is to determine the influence of ambient air humidity and surface wettability on the droplet freezing mechanism. The first part of the paper concerns the droplet deformation scenarios at room temperature to validate the experimental setup. The second part of this work considers the droplet which impinges the surface in icing conditions. The third part deals with influence of preexisting surface frost on the behavior of the droplet (including the experiment with supercooled droplet).

## 2. Experimental setup and investigated surfaces

The experiments were performed using the apparatus shown in Fig. 2. It consisted of a vertical pipe connected to a container inside of which the investigated sample was placed in horizontal position. The casting of a droplet was obtained by means of a specially designed droplet ejection system, capable of producing droplets with diameters in the range of  $d = 0.5 \div 2.2$  mm. Nevertheless, because of the limitations of the optical system this diameter range was narrowed to  $d = 1.9 \div 2.2$  mm. The height of droplet casting was variable allowing to investigate droplet impact at velocity range of  $U = 1.3 \div 3.2$  m/s. The container was transparent so it was possible to observe the investigated phenomenon without image distortion. Recordings were made by means of high-speed camera Photron FASTCAM SA5 with 5000 fps (with maximum resolution of  $1024 \times 1024$  pixels). The measurements of the droplet impact velocity and diameter were done using Photrons software.

The investigated surfaces included steel, aluminum and two specially designed hydrophobic samples. A hierarchical structure, in the first superhydrophobic surface, was created in an epoxy nanocomposite surface by filing the resin with alumina nanoparticles and micron-sized glass beads and subsequently by sand-

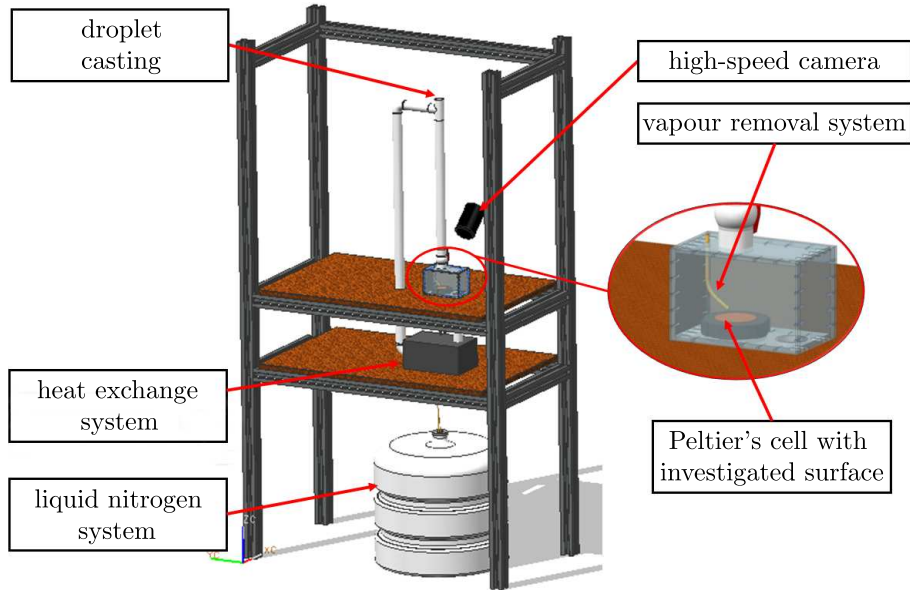
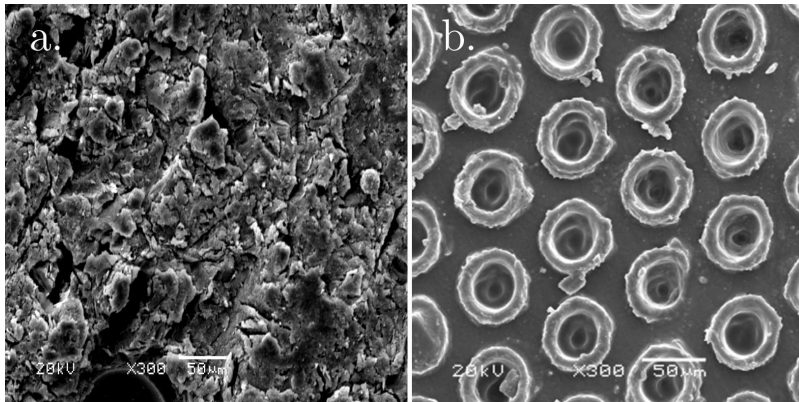


FIG. 2. The experimental stand.

FIG. 3. SEM images of hydrophobic samples: a) superhydrophobic sample (contact angle:  $162^\circ$ ), b) hydrophobic sample (contact angle:  $127^\circ$ ).

blasting with corundum microparticles (see Fig. 3a, PSARSKI *et al.* [25]). The static contact angle of the sample was estimated at  $162^\circ$ . The contact angle hysteresis (CAH) was estimated at  $7 \pm 2^\circ$ . The second hydrophobic sample was manufactured using an aluminum matrix with hexagonal layout of pockets, which was replicated in the epoxy resin mixed with alumina nanoparticles (Fig. 3b). This material was characterized by contact angle  $127^\circ$  and  $CAH = 22 \pm 2^\circ$ .

### 3. Results in the room temperature environment

The purpose of the first part of the research was to validate the setup as well as the measurement techniques. In particular, it was also important to confirm the wetting properties of the investigated surfaces. This was done by comparing our observations with results provided in the literature.

The experiments allowed to distinguish (in hydrophobic and in standard cases) three different phases of motion, as it is described in [13]. The first phase is a so-called kinematic phase, where the diameter increases as  $\sqrt{t^*}$ , the second one is a spreading phase, the third one is a relaxation phase ( $t^*$  denotes a nondimensional time defined as  $t^* = tU/D_0$ ). Differences obtained for various substrates are presented in Figs. 4 and 6 as a function of spread factor (ratio of actual diameter size and droplet impact diameter  $d^* = d/D_0$ ). The analysis was limited to a first phase of impact despite the fact, that for bouncing droplets further oscillations may occur. At early post-impact times thin liquid sheet emerges from the base of the drop [26]. The droplet diameter increases, finally reaching its maximum size. This stage of motion is qualitatively and quantitatively similar for all investigated cases. The only difference is in the value of maximum spread factor, which varies depending on the surface.

In the next relaxation phase, the retraction speed varies depending on surface wetting properties. In this case adhesion forces start to play important role competing with capillary forces. In cases of polished steel and aluminum plates this stage takes much longer time.

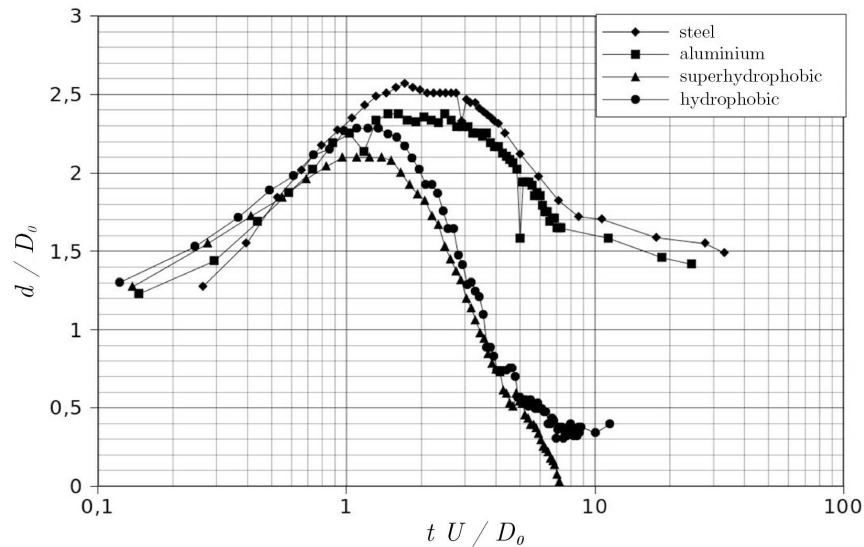


FIG. 4. Spread factor  $d/D_0$  as a function of nondimensional time ( $We = 50 \pm 2$ ).

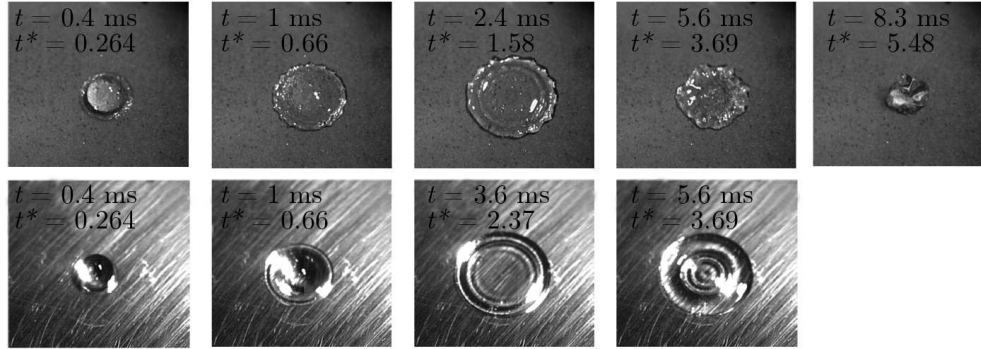


FIG. 5. Water droplet impact ( $We = 50 \pm 2$ ) for superhydrophobic surface (top row) and polished steel substrate (bottom row).

During the relaxation phase, in hydrophobic cases, the velocity of retraction is significantly higher than for the steel and aluminum substrates, which is in agreement with results provided by [13]. The final diameter of the droplet is much higher for metal plates due to higher wettability of these surfaces.

For higher Weber number (Figs. 6 and 7) the kinematic and spreading phases are very similar to the previously described. However, in this case (Fig. 7 top,  $t^* = 1.08$ ) the droplet may lose its axial symmetry as described by RANGE *et al.* [27]. Therefore, only the average diameter can be considered at these stages of motion. This average was estimated as a mean value of the outer diameter related to the fingers and the inner diameter related to the thin liquid film. In contrast to the lower  $We$  number (Figs. 4 and 5) no significant differences were observed between the steel and the aluminum plates. Similarly, the spread factor for all of the investigated surfaces reaches the same maximum.

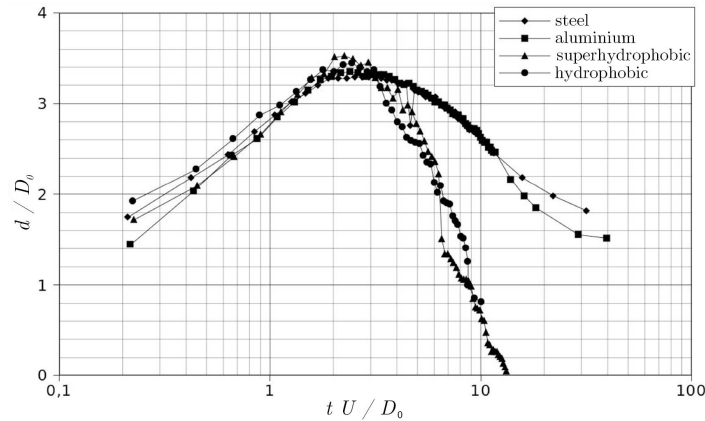


FIG. 6. Spread factor  $d/D_0$  as a function of nondimensional time ( $We = 166 \pm 2$ ).

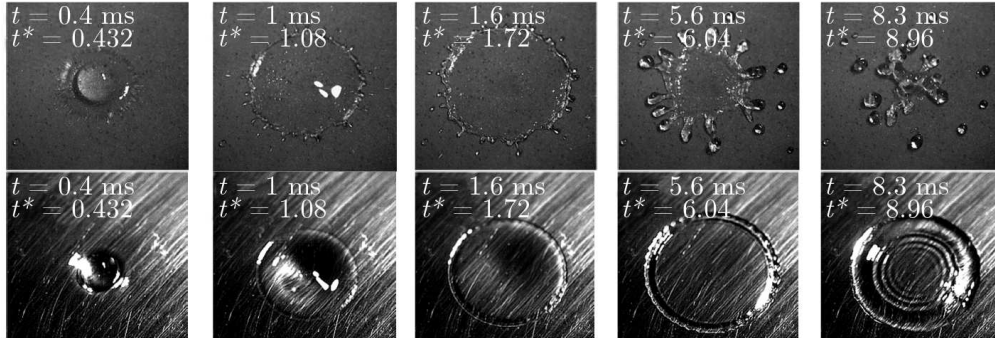


FIG. 7. Water droplet impact ( $We = 166 \pm 2$ ) for superhydrophobic surface (top row) and polished steel substrate (bottom row).

As Weber number grows, time-scale of relaxation stage is shortening. Significant differences between samples were observed in relaxation stage of motion. For hydrophobic samples the droplet was defragmenting into several smaller satellite drops. This phase can also be characterized by partial recoil.

#### 4. Droplet impact under the icing conditions

This part of the research concerned the droplet impacting surfaces with temperature lower than the water freezing point. The experimental setup is presented in Fig. 2. The examined surface was mounted on the top of the Peltier's cell (connected to the cooling system). The temperature of the sample was measured using a thermocouple. The environment temperature remained equal to the room temperature ( $20^{\circ}\text{C}$ ). The relative humidity of air was measured as 75%.

Two surface types were investigated at this stage: polished steel plate and superhydrophobic substrate with contact angle  $162^{\circ}$ . The temperature of the sample was set to  $-10^{\circ}\text{C}$ , while the temperature of a liquid (deionized water) was the same as of the environment ( $20^{\circ}\text{C}$ ). It should be noted that for the 75% relative air humidity at  $20^{\circ}\text{C}$ , the temperature  $-10^{\circ}\text{C}$  remains well below the dew point. These conditions correspond to a high humidity ambient cold atmosphere for an aircraft. The spread factor during the impact as a function of nondimensional time is shown in Figs. 9 and 10. For both Weber numbers a higher maximum value of the spread factor was observed for droplets impinging the superhydrophobic sample. This can be explained by different thermal properties of both surfaces (more ice is created on the metallic surface). As  $We$  is increased, the difference becomes more evident. It could be also noticed that the formation of ice layer is slowing down the droplet spreading, that is the maximum of  $d/D_0$  is reached at a later time  $tU/D_0$  for the cold substrate.

However, after reaching the maximum diameter, there is no retraction. The layer of liquid, which remained in contact with the surface becomes frozen (Fig. 8).

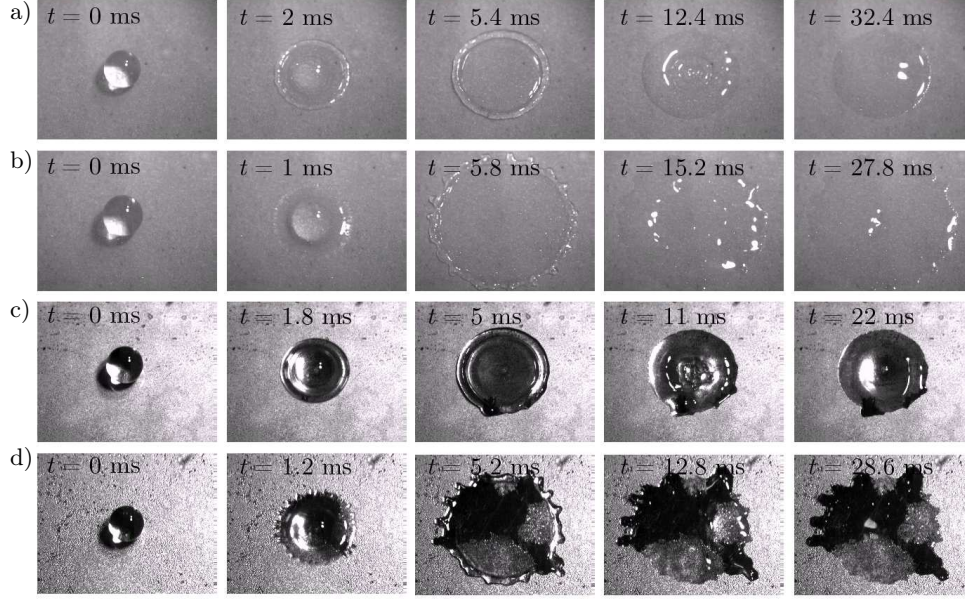


FIG. 8. Droplet freezing process. Time elapsed images of water droplet impingement for superhydrophobic surface: a)  $We = 50 \pm 2$ , b)  $We = 166 \pm 2$  and polished steel substrate: c)  $We = 50 \pm 2$ , d)  $We = 166 \pm 2$ .

To better understand the process of freezing, a very simple model was considered. First the spreading time  $\tau_d = D_0/U$  was compared to the characteristic time  $\tau_s = h^2/\alpha$  related to the heat exchange process at the surface ( $h$  denotes the thickness of the surface, while  $\alpha = \lambda/\rho \cdot c_p$  stands for the thermal diffusivity coefficient). In our experiment, the former is by several orders of magnitude lower than the latter one ( $\tau_d \sim 10^{-3}$  s,  $\tau_s \sim 10^2$  s). It means that in the timescale of the collision, during which the heat transfer process is considered, the surface behaves as a semi-infinite half-space.

Therefore, the maximum possible heat flux through the surface can be well described as [28]:

$$(4.1) \quad q(t) = \sqrt{\frac{\rho c_p \lambda}{\pi t}} \Delta T,$$

where  $\rho c_p$  stands for thermal capacity per unit volume, while  $\Delta T$  denotes the temperature difference between the surface and the water film.

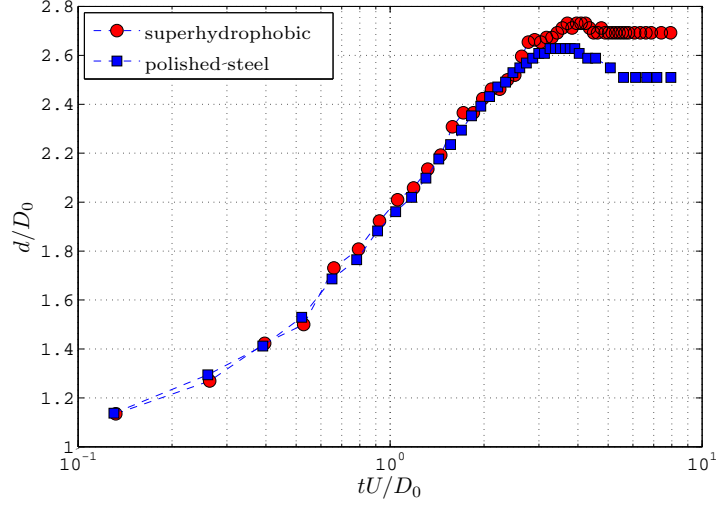


FIG. 9. Spread factor  $d/D_0$  as a function of time for  $We = 50 \pm 2$  (droplet becomes frozen as it reaches maximum diameter; temperature of the surface:  $T_s = -10^\circ\text{C}$ ).

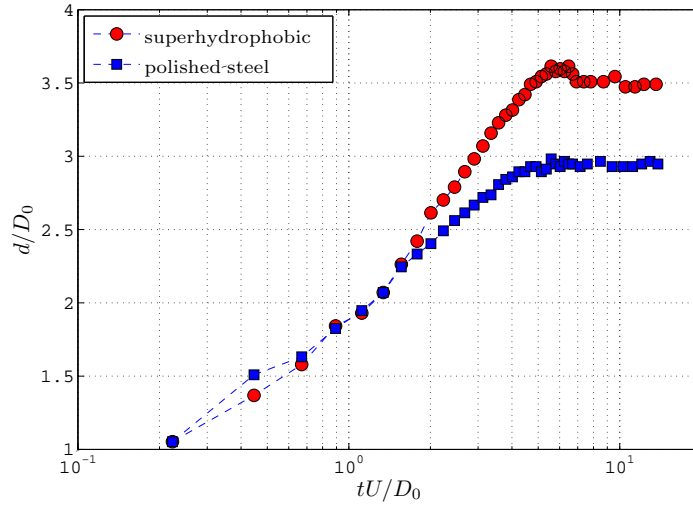


FIG. 10. Spread factor  $d/D_0$  as a function of time for  $We = 166 \pm 2$  (droplet becomes frozen as it reaches maximum diameter; temperature of the surface:  $T_s = -10^\circ\text{C}$ ).

The maximum energy transferred due to this process in the time interval  $t \in \langle 0, \tau_d \rangle$  can be therefore estimated as

$$(4.2) \quad Q = S \int_0^{\tau_d} q(t) dt = 2S \sqrt{\rho c_p \lambda} \Delta T \cdot \frac{\sqrt{\tau_d}}{\sqrt{\pi}},$$

where  $S$  denotes the spreading area of the droplet. This quantity can be approximated in our experiment as  $\sim 0.01$  J for epoxy resin and as  $\sim 0.1$  J for stainless steel.

The energy, that has to be retrieved in order to freeze the droplet, can in turn be estimated in our experiment as

$$(4.3) \quad Q_f = \frac{\pi D_0^3}{6} \rho_f \cdot L \sim 2 \text{ J}$$

where  $L$  is the latent heat of water ( $L = 334$  kJ/kg). Comparing (4.2) and (4.3) it is possible to roughly predict the solidified fraction of water droplet as

$$(4.4) \quad \eta = \frac{Q}{Q_f} = \frac{\rho}{\rho_f} \text{Ste} \cdot \sqrt{\frac{\tau_d \alpha}{\pi}} \frac{S}{V},$$

where  $V = \pi D_0^3/6$  is the volume of droplet, while  $4\sqrt{\tau_d \cdot \alpha}$  can be interpreted [28] as the thermal penetration thickness. In the experiment,  $\eta = 0.005$  and  $\eta = 0.05$  for the superhydrophobic surface and for the steel surface respectively.

Therefore, for both surfaces only the partial freezing of water is possible (in the spreading phase). From Eq. 4.2 it can be additionally inferred, that it is the value of  $\rho c_p \lambda$  (characterizing the surface) which is responsible for larger spreading diameter of the droplet on the superhydrophobic surface – see Figs. 9 and 10 (less ice is created on such surface). The value of  $\rho c_p \lambda$  can be estimated as  $0.49 \cdot 10^6 \left[ \frac{\text{W}^2 \cdot \text{s}}{\text{m}^4 \cdot \text{K}^2} \right]$  and  $64 \cdot 10^6 \left[ \frac{\text{W}^2 \cdot \text{s}}{\text{m}^4 \cdot \text{K}^2} \right]$  for the epoxy superhydrophobic surface and for the steel surface respectively. However, further experimental studies are necessary to fully understand this phenomenon and in particular the influence of the Weber number – which cannot be explained by the present argument.

To determine why, despite of superhydrophobic properties of the surface, the droplet starts to freeze already in the spreading phase additional experiments were performed. In the first one, the sample was kept for 300 seconds in the same environment as it was in the case of droplet impingement. The temperature of substrate was kept at constant level of  $-10^\circ\text{C}$ . It was observed that sample becomes covered with substantial amount of frost (Fig. 11). Apparently, the process of ice accumulation on the investigated substrate runs relatively fast.

To verify that indeed the frost is responsible for triggering the droplet freezing during the spreading phase, another experiment was performed, in which the entire system was filled up with vapour-free nitrogen gas, kept at room temperature (relative humidity inside the system was measured as 9%). In addition, to dispose of water vapour from the pores of the surface, the direct, vapour-free nitrogen blowing system was used. The investigated surface was cooled down

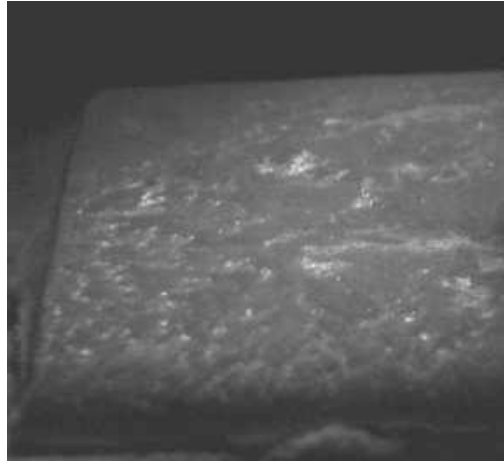


FIG. 11. Example of frosting on hydrophobic surface.

by means of Peltier's cell. In Fig. 12b it can be observed that the droplet does not freeze and the process of deformation is the same as in the case of room temperature experiments (Fig. 12a). One can suspect then, that the lack of ice crystal nuclei (present in the frost) allows for effective prevention/delay of icing. In addition, the frost filling all imperfections of the surface may actually increase the heat transfer between the droplet and the surface.

This experiment seems to indicate that the freezing process cannot be easily prevented if the surface itself is already covered by frost. Condensation of vapour and subsequent freezing leads to the creation of a thin layer of ice, which changes the heat transfer properties of the surface. Presence of the ice increases thermal conductivity, which eventually leads to the droplet freezing.

It is important to confirm this result also for the initially supercooled droplets, as this is an extremely important range for aeronautic applications (see TABAKOVA *et al.* [29] for theoretical modelling). To investigate this case the set up shown in Fig. 2 was filled with vapour-free gaseous nitrogen. The gas inside the system was cooled by means of a heat exchange system, inside of which liquid nitrogen circulated (switched-off just prior to the experiment). The temperature was determined (using thermocouples) at several points of the system. The temperature of liquid inside the syringe was measured to be  $-10^{\circ}\text{C}$ . The height of casting was 1.2 m. As the droplet hits the surface, all stages of motion are very similar to what was earlier observed at room temperature experiments (see Figs. 12c, 12d and 12a for comparison). It confirms the earlier hypothesis that indeed surface frost is responsible for droplet freezing at the early stage of the process for this range of experimental parameters. It seems also that in this range of parameters the elimination of frost is a necessary condition for the delay of icing.

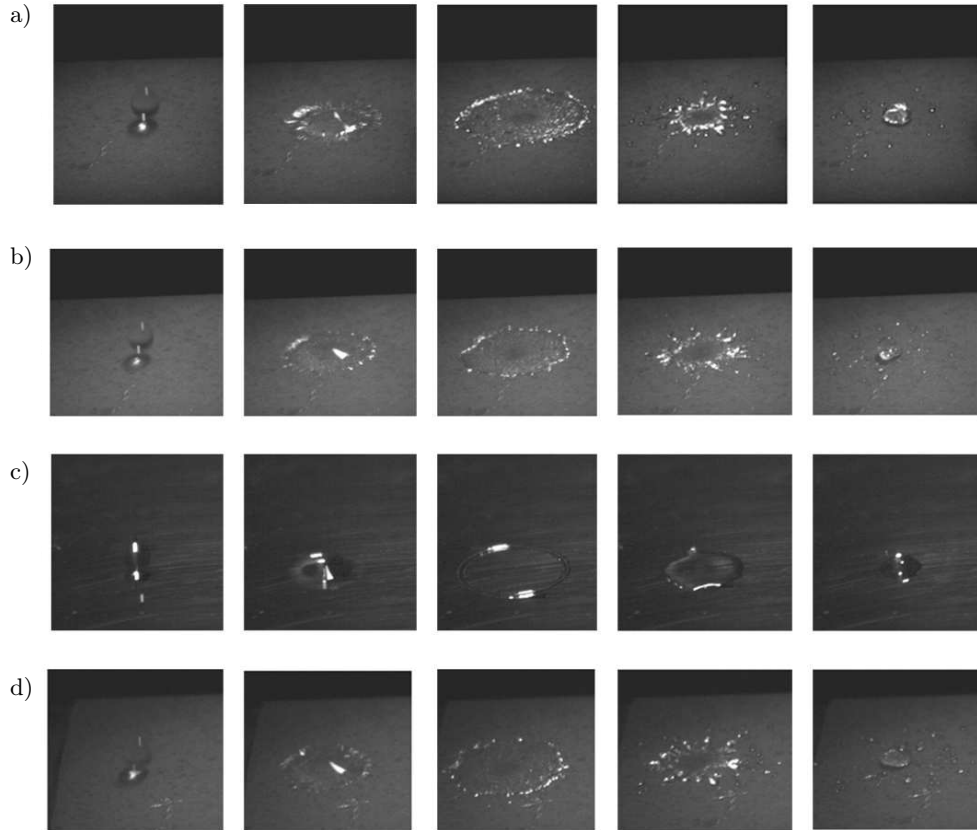


FIG. 12. Influence of the temperature difference between the surface  $T_S$  and the droplet  $T_d$  on the impact scenario: a) hydrophobic  $T_S = T_d = 20^\circ\text{C}$ ; b) hydrophobic,  $T_S = -15^\circ\text{C}$ ,  $T_d = 20^\circ\text{C}$ ; c) steel,  $T_S = -15^\circ\text{C}$ ,  $T_d = 20^\circ\text{C}$ ; d) superhydrophobic,  $T_S = T_d = -10^\circ\text{C}$ .

## 5. Conclusions

The present paper dealt with investigation of droplet impact on surfaces with different wetting properties and in the icing conditions. The first part consisted in validation of wetting properties of the surfaces in the ambient temperature environment. Validation of the experimental setup was performed by comparing the observations related to the droplet impact with those obtained by other authors.

Different phases of motion have been distinguished. The first and the second, the so-called kinematic and spreading phases respectively, are the same for all of the investigated cases. Just after impact, the droplet spreads reaching the final diameter. No significant differences in the spreading velocity have been

noticed at these stages. In case of hydrophobic substrates the spreading phase is characterized by appearance of fingers.

The next phase of the droplet motion, the so-called relaxation, is governed by surface tension and adhesion forces at the droplet boundary. Retraction velocity in superhydrophobic case is higher than for steel or aluminum substrate. All observations are consistent with previous works of other authors.

The main part of the research, presented in this paper, considered the passive anti-icing application of hydrophobic surfaces. In humid-air environment, the droplet impacting the surface with the temperature  $T_S < 0^\circ\text{C}$  starts to freeze as it reaches the maximum diameter (independently of surface properties). When the vapour inside the system is eliminated, the droplet does not freeze while the deformation scenario remains the same as in the room temperature experiments.

Therefore, it can be concluded that condensation and subsequent freezing of vapour inside the pores of the substrate compromise anti-icing application of hydrophobic surfaces. This conclusion is strengthened by the experiment in which the supercooled droplet impacts the cold surface. In this case again, the droplet does not freeze if the experiment is conducted in vapour-free environment. It seems therefore that, within the range of investigated parameters, the crucial factor for controlling the droplet freezing process is the existence of water vapor in the system. To our knowledge this is the first time that such an observation was presented.

### Acknowledgements

This work was supported by the Polish Ministry of Science and Higher Education through research project 2222/B/T02/2009/37 as well as by the "Diamond Grant" programme (DI 2011 002241).

### References

1. A.M. WORTHINGTON, *On the forms assumed by drops of liquids falling vertically on a horizontal plate*, Proceedings of the Royal Society of London, **25**, 261–272, 1876.
2. H. LIU, *Science and Engineering of Droplets, Fundamentals and Applications*, Noyes Publications, New York, USA, 2000.
3. M. REIN, J.P. DELPLANQUE, *The role of air entrainment on the outcome of drop impact on a solid surface*, Acta Mechanica, **201**, 105–118, 2008.
4. A.L. YARIN, *Drop impact dynamics: splashing, spreading, receding, bouncing, . . .*, Annual Review of Fluid Mechanics, **38**, 159–192, 2006.
5. C. CLANET, C. BEGUIN, D. RICHARD, D. QUERE, *Maximal deformation of an impacting drop*, Journal of Fluid Mechanics, **517**, 199–208, 2004.

6. D. BARTOLO, C. JOSSE RAND, D. BONN, *Retraction dynamics of aqueous drops upon impact on non-wetting surfaces*, Journal of Fluid Mechanics, **545**, 329–338, 2005.
7. F. CHEVY, A. CHEPELIANSKII, D. QUERE, E. RAPHAEL, *Liquid Hertz contact: Softness of weakly deformed drops on non-wetting substrates*, Europhysics Letters, **100**, (5), 54002, 2012.
8. S. YUN, J. HONG, K.H. KANG, *Suppressing drop rebound by electrically driven shape distortion*, Physical Review E, **87**, (3), 2013.
9. K. OKUMURA, F. CHEVY, D. RICHARD, D. QUERE, C. CLANET, *Water spring: A model for bouncing drops*, Europhysics Letters, **62**, (2), 237–243, 2003.
10. K.K. VARANASI, T. DENG, M. HSU, N. BHATE, *Hierarchical superhydrophobic surfaces resist water droplet impact*, Technical Proceedings of the 2009 NSTI Nanotechnology Conference and Expo, 2009.
11. D. BARTOLO, F. BOUMRIRENE, E. VERNEUIL, A. BUGUIN, P. SILBERZAN, S. MOULINET, *Bouncing or sticky droplets: Impalement transitions on superhydrophobic micropatterned surfaces*, Europhysics Letters, **74**, (2), 299–305, 2006.
12. S.F. LUNKAD, V.V. BUWA, K.D.P. NIGAM, *Numerical simulations of drop impact and spreading on horizontal and inclined surfaces*, Chemical Engineering Science, **62**, (24), 7214–7224, 2007.
13. R. RIOBOO, M. MARENGO, C. TROPEA, *Time evolution of liquid drop impact onto solid, dry surfaces*, Experiments in Fluids, **33**, 112–124, 2002.
14. L. ZHANG, R.D. DEEGAN, P. BRUNET, J. EGGERS, *Wavelength selection in the crown splash*, Physics of Fluids, **22**, 122105, 2010.
15. L. XU, W.W. ZHANG, S.R. NAGEL, *Drop splashing on a dry smooth surface*, Physical Review Letters, **94**, (184505), 1–4, 2005.
16. D. GUEYFFIER, S. ZALESKI, *Finger formation during droplet impact on a liquid film*, Comptes Rendus de l’Academie des Sciences, Series IIB Mechanics Physics Astronomy, **326**, 839–844, 1998.
17. R. KRECHETNIKOV, G.M. HOMS Y, *Crown-forming instability phenomena in the drop splash problem*, Journal of Colloid and Interface Science, **331**, 555, 2009.
18. A.L. YARIN, D.A. WEISS, *Impact of drops on solid surfaces, selfsimilar capillary waves, and splashing as a new type of kinematic discontinuity*, Journal of Fluid Mechanics, **283**, 141, 1995.
19. M.M. DRISCOLL, S.R. NAGEL, *Ultrafast Interference imaging of air in splashing dynamics*, Physical Review Letters, **107**, 2011.
20. S. JUNG, M.K. TIWARI, D. POULIKAKOS, *Frost halos from supercooled water droplets*, Proceedings of the National Academy of Sciences of the United States of America, **109**, (40), 16073–16078, 2012.
21. H. WANG, L. TANG, X. WU, W. DAI, Y. QIU, *Fabrication and anti-frosting performance of super hydrophobic coating based on modified nano-sized calcium carbonate and ordinary polyacrylate*, Applied Surface Science, **253**, (22), 8818–8824, 2007.
22. S.A. KULINICH, S. FARHADI, K. NOSE, X. W. DU, *Superhydrophobic surfaces: are they really ice-repellent?*, Langmuir, **27**, (1), 25–29, 2011.

23. S.A. KULINICH, M. FARZANEH, *How wetting hysteresis influences ice adhesion strength on superhydrophobic surfaces*, *Langmuir*, **25**, (16), 8854–8856, 2009.
24. K. RYKACZEWSKI, S. ANAND, S.B. SUBRAMANYAM, K.K. VARANASI, *Mechanism of frost formation on lubricant-impregnated surfaces*, *Langmuir*, **29**, (17), 5230–5238, 2013.
25. M. PSARSKI, J. MARCZAK, G. CELICHOWSKI, G. SOBIERAJ, K. GUMOWSKI, F.L. ZHOU, *Hydrophobization of epoxy nanocomposite surface with 1H,1H,2H,2H-perfluorooctyltrichlorosilane for superhydrophobic properties*, *Central European Journal of Physics*, **10**, (5), 1197–1201, 2012.
26. A. MONGRUEL, V. DARU, F. FEUILLEBOIS, S. TABAKOVA, *Early post-impact time dynamics of viscous drops onto a solid dry surface*, *Physics of Fluids*, **21**, 032101, 2009.
27. K. RANGE, F. FEUILLEBOS, *Influence of surface roughness on liquid drop impact*, *Journal of Colloid and Interface Science*, **203**, 16–30, 1998.
28. R.B. BIRD, W.E. STEWART, E.N. LIGHTFOOT, *Transport Phenomena*, John Wiley & Sons, Inc., 2002.
29. S. TABAKOVA, F. FEUILLEBOIS, *On the solidification of a supercooled liquid droplet lying on a surface*, *Journal of Colloid and Interface Science*, **272**, 225–234, 2004.

*Received September 11, 2013; revised version January 17, 2014.*

---